2021

Direct multiplexing of low order aberration modes in a photopolymerbased holographic element for analog holographic wavefront sensing

Emma Branigan
Technological University Dublin, emma.branigan@tudublin.ie

Suzanne Martin
Technological University Dublin, suzanne.martin@tudublin.ie

Matthew Sheehan
Technological University Dublin, matthew.sheehan@tudublin.ie

Recommended Citation

Emma Branigan, Suzanne Martin, Matthew Sheehan, Kevin Murphy, "Direct multiplexing of low order aberration modes in a photopolymer-based holographic element for analog holographic wavefront sensing," Proc. SPIE 11860, Environmental Effects on Light Propagation and Adaptive Systems IV, 118600H (12 September 2021); doi: 10.1117/12.2599912

Funder: Science Foundation Ireland

Direct multiplexing of low order aberration modes in a photopolymer-based holographic element for analog holographic wavefront sensing

Branigan, Emma, Martin, Suzanne, Sheehan, Matthew, Murphy, Kevin

Emma Branigan, Suzanne Martin, Matthew Sheehan, Kevin Murphy, "Direct multiplexing of low order aberration modes in a photopolymer-based holographic element for analog holographic wavefront sensing," Proc. SPIE 11860, Environmental Effects on Light Propagation and Adaptive Systems IV, 118600H (12 September 2021); doi: 10.1117/12.2599912

SPIE.

Event: SPIE Remote Sensing, 2021, Online Only

Direct multiplexing of low order aberration modes in a photopolymer-based holographic element for analog holographic wavefront sensing

Emma Branigan[1], Suzanne Martin[1], Matthew Sheehan[2], Kevin Murphy[1]

1. Centre for Industrial and Engineering Optics, School of Physics and Clinical & Optometric Sciences, TU Dublin
2. School of Physics and Clinical & Optometric Sciences, TU Dublin

ABSTRACT

The fabrication of an analog holographic wavefront sensor, capable of detecting the low order defocus aberration, was achieved in an acrylamide-based photopolymer. While other implementations of holographic wavefront sensors have been carried out digitally, this process utilises a recording setup consisting only of conventional refractive elements so the cost and complexity of holographic optical element (HOE) production could be much reduced. A pair of diffraction spots, corresponding to a maximum and minimum amount of defocus, were spatially separated in the detector plane by multiplexing two HOEs with different carrier spatial frequencies. For each wavefront with a known aberration that was introduced during playback of the hologram, the resulting intensity ratio was measured in the expected pair of diffracted spots. A number of HOEs were produced with the diffraction efficiency of the multiplexed elements equalized, for a range of diffraction efficiency strengths, some as low as <5%. These HOEs were used to successfully classify four amounts of the defocus aberration through the observed intensity ratio.

Keywords: Wavefront sensing, analog holographic wavefront sensor, holography, adaptive optics, ophthalmology

1. INTRODUCTION

Wavefront sensors (WFS) are devices used in the detection of aberrations or optical anomalies of a wavefront. A common example of a WFS is the Shack-Hartmann WFS (SHWFS), comprised of a micro lens array and a detector[1]. Integration of the local slope distribution gives a measure of the aberration present in an incident wavefront[2]. The SHWFS has become the most widely appliedWFS for the detection of both low and higher order ocular aberrations (e.g. defocus, coma) in routine human-eye measurements[3] and in procedures such as laser refractive surgery[4]. In operational principle the SHWFS is simple and robust but is reliant on costly high-resolution imaging equipment and computationally expensive algorithms necessary for highly-accurate wavefront fitting. The bulky nature and price of these instruments typically restrict their use to specialist clinics.

It is advantageous to construct a WFS that is highly efficient, cost-effective and applicable in a wide variety of environments such as ophthalmology[5], optical communications[6] and astronnomy[7]. Analog Holographic Wavefront Sensors (AHWFS) have previously been achieved by recording various aberration modes in both dichromated gelatin[8] (DCG) and silver halide[9,10]. These implementations of AHWFS were achieved using digital holographic recording techniques by producing computer generated holograms of the aberration modes using a Spatial Light Modulator (SLM). Unlike the SHWFS, AHWFS are insensitive to both scintillation and local obscuration making them suitable to the turbulent environments often faced in many long range or highly discontinuous sensing applications[11]. When a wavefront containing arbitrary aberration modes is incident on the device, they will be optically decomposed into a set of paired diffracted beams for each mode. A normalized ratio of intensities at an array of photodetectors will determine the magnitude of the aberration[12,13], while the angular position can be used to determine the aberration type, at speeds limited only by the detector readout. In theory, bandwidth in the megahertz range will be achievable using commercially available and inexpensive photodetectors. The design of this WFS omits the need for costly high-resolution imaging equipment and greatly reduces the computational overhead required for wavefront fitting.

Environmental Effects on Light Propagation and Adaptive Systems IV, edited by Karin Stein, Szymon Gladysz, Proc. of SPIE Vol. 11860, 118600H · © 2021 SPIE
CCC code: 0277-786X/21/$21 · doi: 10.1117/12.2599912

Here we seek to record an AHWFS in an acrylamide-based photopolymer which is self-developing and mass producible[14]. The reproducibility and chemical post-processing and developing of materials such as silver halide and DCG are some of the major material challenges that can be avoided when recording multiplexed holographic optical elements (HOE) in photopolymers. Typically, DCG's poor robustness to moisture can cause problems for the recorded holograms shelf life and some of the chemicals used in its preparation and processing have a high level of toxicity. Shrinking, swelling and distortion of holograms recorded in DCG and silver halide materials can occur during the development process. High reproducibility, from one volume hologram to the next, can be achieved in the photopolymer without the need for any chemical post-processing step. Good dynamic range of the material will facilitate multiplexing of a number of modes into one HOE, allowing many aberrations to be detectable simultaneously. This is beneficial when developing a multi-functional device that will be applicable in a variety of settings.

The Materials and Methods section describes the preparation of the photopolymer layer used to record the HOEs and the optical setups and methodology utilised for the recording and reconstruction of the holograms. The Measurement of the Defocus Aberration section details the characteristics of the HOEs recorded and provides results for their use in detecting defocus aberration. The Summary and Conclusions section outlines the key achievements and results obtained from the AHWFS fabricated as part of this work.

2. MATERIALS AND METHODS

2.1 Material and sample preparation

A 10% w/w stock polyvinyl alcohol (PVA) solution and a stock dye solution with a concentration of 1.1mg/cm^3 of Erythrosine B, both in water, were prepared. Then 2.0ml of triethanolamine, 0.2g of bisacrylamide and 0.8g of acrylamide monomers[15] were added to 17.5ml of the PVA solution. Finally, 4ml of stock dye solution was added. The mixture was stirred continuously until all of the monomers dissolved.

An appropriate volume of photopolymer solution was carefully pipetted out onto a 75 x 25mm glass slide and left to dry on a levelled plate for 24-36 hours. A wet volume of 657µL, spread on the slide, gave a dry layer of nominal 65.7 ± 12.14µm thickness as shown in Figure 1. Some thickness variation, from layer to layer, was observed. This was probably due to variations in how level the sample was during drying and local thickness variations introduced during the drying process. Once dry, the layer was preserved and protected from changes in humidity and temperature by covering with a 125µm layer of Lexan 8010 polycarbonate film.

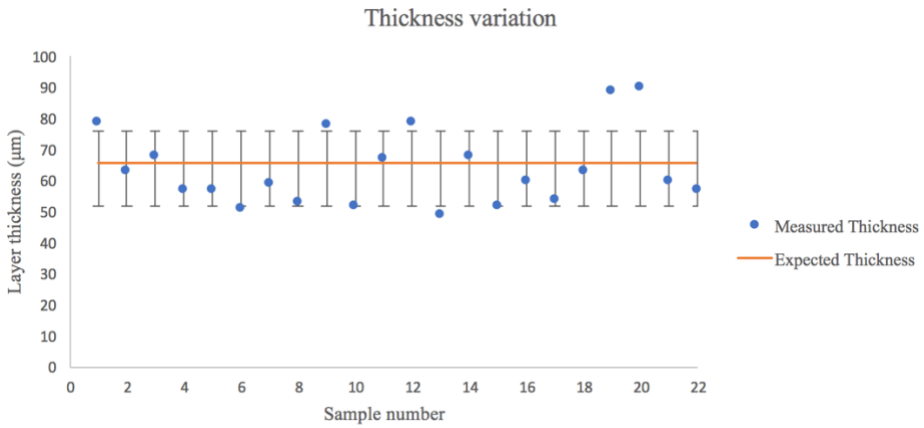

Figure 1. The thickness of a number of samples, measured close to the site of the recorded HOEs. The thickness of the photopolymer layer was determined by: total thickness - cover film - slide thickness using a micrometer.

2.2 Holographic recording

In order to make the HWFS, recording of a volume Bragg HOE, by transmission holography, was carried out at a wavelength of 532nm with a Nd:YAG laser. The spatially filtered beam was collimated and directed towards the photopolymer sample using a beam splitting system as shown in Figure 2. The photopolymer holographic recording material was fixed in place with the covered photopolymer layer facing the surface of the beam splitter. The incident beam from the reference arm was reflected back along its path to ensure that it was normal to the surface of the recording material. A biconvex-refractive lens with a focal length of 150mm (L1) was mounted in the reference arm of the recording setup to produce the defocus aberration. An aperture reduced the diameter of the collimated object beam to 4mm to fully overlap with the reference beam, producing the interference pattern required to record the appropriate pattern within the photopolymer

Two locations along a rail, a distance away from the sample, were chosen to generate a maximum (217mm from the sample) and minimum (83mm from the sample) phase delay/advance of the defocus mode. The result was the separate recording of a holographic converging lens ($L1_{min}$) and a holographic diverging lens ($L1_{max}$) in the photopolymer layer with focal lengths of 67mm. This produced an equal and opposite amount, ±15.0D, of defocus aberration for the two holographic lenses over a diameter of 4mm. It was necessary to multiplex the hologram as a new recording was required to correspond with both limit positions of the refractive lens i.e. for every phase delay associated with the chosen mode of wavefront aberration. All optical components were clamped tightly in place to the bench and rail to ensure any vibrational disturbance was kept to a minimum.

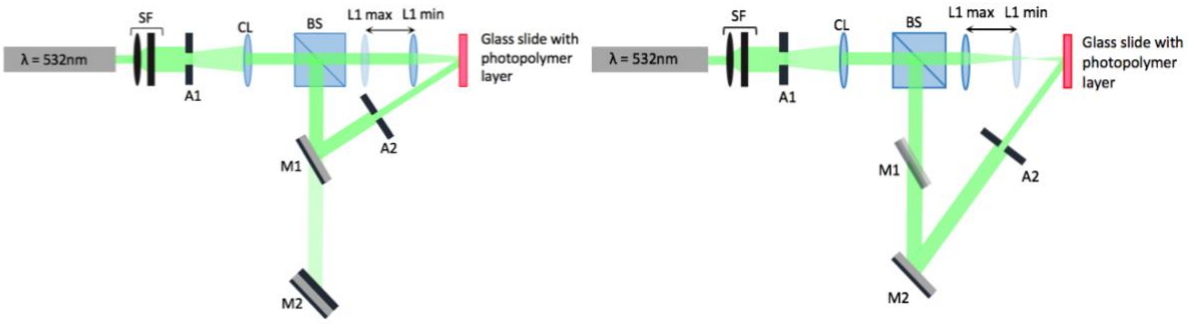

Figure 2a. (left) & 2b. (right) Recording setup to multiplex a HOE with a maximum and minimum amount of the defocus aberration at 497 lines/mm (left) and 816 lines/mm (right), where the optical components shown are as follows: SF: spatial filter; A1: 1mm aperture; CL: collimating lens; BS: beam splitter; L1: 150mm spherical refractive lens; M1 & M2: planar mirrors; A2: 4mm aperture.

Angular multiplexing techniques were employed to separate the diffracted output of the holographic lenses. The object beam was first reflected off a plane mirror at an angle of 15.3° (Fig 2a.) to record holographic grating 1 (HG1). The spatial frequency range across the horizontal axis of lens element was calculated using geometry and the diffraction grating equation (Eq. 1, where d: grating spacing; θ: interbeam angle; m: diffraction order; λ: recording wavelength) as 442-551 lines/mm, with a carrier spatial frequency of 497 lines/mm. The first mirror was then removed, and a second mirror was used to introduce a subsequent grating (HG2) with a spatial frequency range of 763-868 lines/mm and a carrier spatial frequency of 816 lines/mm, interfering with the reference beam at an angle of 25.4° (Fig 2b.). The minimum and maximum amounts of the defocus aberration were recorded in HG1 and HG2 respectively. As the holographic gratings (HG1 and HG2) are volume Bragg gratings diffraction will only occur in the first order once each specific Bragg condition has been satisfied.

$$2d\sin\theta = m\lambda \qquad \text{(Equation 1)}$$

An electromechanical shutter controlled the exposure time of the layer to the laser to achieve a desired diffraction efficiency (DE). Laser intensity equivalent to 0.28mW/cm^2 was delivered to the sample. A short delay (~30s) was introduced between the recordings at HG1 and HG2 as M1 was removed from the setup manually and L1 was positioned along the rail. In general, a longer exposure time was needed to record HG2 as some of the dynamic range of the photopolymer had been depleted during the first recording. It was necessary to bleach the samples with a high UV dose after recording, in particular for those with a very low DE, in order to fully polymerise any remaining monomer in the layer.

2.3 Hologram reconstruction

Careful realignment of the sample in the holder was needed to ensure correct reconstruction of the HOE. The sample was clamped in place in the same orientation used in recording i.e. with the photopolymer layer facing towards the beam splitter. The object arm of the setup was baffled for the purpose of replaying the hologram, so that only the beam in the reference arm was incident on the sample. When L1 was moved along the reference arm rail to the minimum position, the collimated beam at HG1 was observed at the diffracted angular position corresponding to HG1. This reconstructed the object beam and indicated that the incident probe beam was Bragg matched to the recording reference beam for HG1. In a perfectly efficient system 100% of the incident light would be diverted into this collimated beam, however it was observed that a fraction of the incident beam was always also diffracted into a diverging spot at HG2. At the maximum position on the rail, the opposite was true. It was seen that a collimated beam formed in the HG2 location, while some light was also present at HG1.

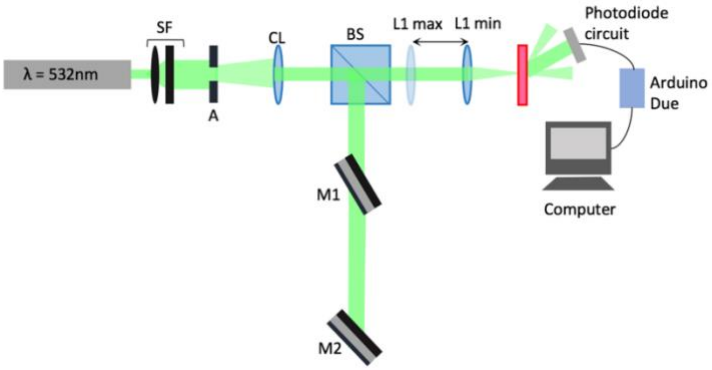

Figure 3. Reconstruction of the HOE, where the object beam was baffled and only the reference beam was incident on the sample. A photodiode circuit, Arduino Due and a computer serial monitor were used in measuring the diffraction efficiency and normalized intensity ratio of each recording.

A silicon PIN photodiode (VEMD5510CF), connected to the analog input of an Arduino Due was used to measure the diffraction efficiency of each recording. L1 was moved into the minimum position along the rail and the power was measured in the HG1 spot. The diode was moved into the HG2 spot, where the beam filled the entirety of the detector area. The power in the transmitted beam was measured in the same way. The diffraction efficiency of the HG1 recording was then calculated by Eq. 2. This process was repeated with L1 in the maximum position to measure the efficiency of the HG2 recording (Eq. 3).

$$\text{Diffraction Efficiency}_{HG1} = \frac{I_{HG1}}{I_{HG1} + I_{HG2} + I_T} * \frac{100}{1} \qquad \text{(Equation 2)}$$

$$\text{Diffraction Efficiency}_{HG2} = \frac{I_{HG2}}{I_{HG2} + I_{HG1} + I_T} * \frac{100}{1} \qquad \text{(Equation 3)}$$

A normalized ratio of intensities (Eq. 4) between the HG1 and HG2 spots was used to determine the amount of an aberration present in the incident wavefront. In a fixed plane, a detector with an aperture set to 4mm diameter, to match the size of the collimated beam, measured the intensity difference between the two spots.

$$\text{Normalized Intensity Ratio} = \frac{I_{HG1} - I_{HG2}}{I_{HG1} + I_{HG2}} \qquad \text{(Equation 4)}$$

The detectable range of the HOE was quantified in dioptres as: 1/focal length of the HOE (in metres). The focal length of the holographic lenses (HG1 and HG2) was measured by illuminating the HOE with the collimated beam in the object arm, at the Bragg angle for each grating, i.e. at 15.3° for HG1 and at 25.4° for HG2. The focal length of HG1 was measured with the photopolymer layer facing into the incident beam. This reconstructed the converging lens that was recorded for $L1_{min}$. The distance between the HOE and the focal spot was measured as 67mm. In order to measure the focal length of HG2, the HOE was rotated so that the photopolymer layer was now on the back surface of the slide – facing away from the beam. This was necessary to reconstruct the focus of the diverging lens that was recorded for $L1_{max}$. As before, HG2 was then illuminated with the collimated beam at the corresponding reconstruction angle and the distance between the sample and focus was measured as 67mm also. The sign convention is important here to correctly determine whether the amount of defocus present is positive or negative so we express the focal length of the diverging lens as -67mm.

Taking the measured focal length for each holographic lens, the total detectable range of the HOE was ±15.0D. For wavefronts with an unknown amount of defocus, it was possible to determine the strength of the aberration through the above normalized intensity ratio (NIR). In order to classify the aberration, defocus in this case, in terms of the range of the HOE the NIR was expressed in dioptres as follows:

$$\text{Defocus, in dioptres} = \text{NIR} * 15.0\text{D} \qquad \text{(Equation 5)}$$

3. MEASUREMENT OF THE DEFOCUS ABERRATION

3.1 Diffraction efficiency and normalized intensity ratio measurements

The reconstructed spots for the multiplexed HOE can be seen in Figure 4. For $L1_{min}$ (Fig. 4a) the collimated beam was reconstructed in the corresponding angular position associated with HG1, while the transmitted beam focussed to a point. At the diffraction angle corresponding to HG2 a diverging beam was observed, with some noise present. In a perfect system, no light would be diffracted into the HG2 position, for the $L1_{min}$ condition, resulting in a normalized intensity ratio between HG1 and HG2 of exactly 1. At $L1_{max}$ (Fig. 4b), the collimated beam was reconstructed at the HG2 angular position, as expected while HG1 and the transmitted beam were both diverging. This time some unwanted light was diffracted into the HG1 spot which, as mentioned, slightly impacted the intensity ratio that was observed between HG2 and HG1.

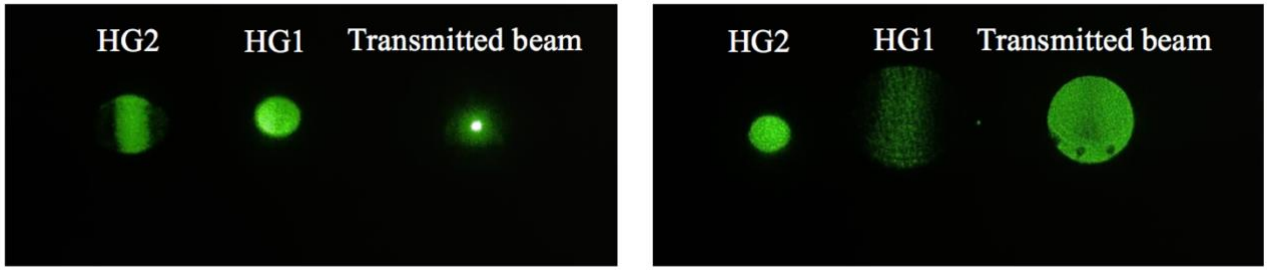

Figure 4a. (left) & 4b. (right) Reconstructed diffraction spots at the output positions for HG1 and HG2, while the probe beam has the lens in the (a) minimum and (b) maximum lens positions.

It was possible to measure the DE of each recording, for each individual HOE. During reconstruction of the hologram, a photodiode was used to measure the power in both the HG1 and HG2 spots, along with the transmitted beam as discussed in section 2.3. It was desirable to try to control the strength and equalize the diffraction efficiencies of the two recordings at HG1 and HG2 to achieve an NIR that was as equal and opposite for the $L1_{min}$ and $L1_{max}$ replay conditions, and as close to ±1 as possible. This was carried out by first recording a number of single element HG1 gratings and measuring the DE achieved for recordings at various exposure times. When multiplexing, some of the dynamic range of the material is used up during the recording of HG1 so a longer exposure time for HG2 is necessary. For this reason, DE equalization was carried out through an iterative process guided by DE measurements of the recorded holograms.

The average diffraction efficiency of HG1 and HG2 was calculated for each sample and are shown in Figure 5. The targeted diffraction efficiency ranges were 35-40%; 20-25%; 5-10%; and <5%. An acceptable DE equalization range was calculated as ±20% of this average. Equalization of DE between HG1 and HG2 was important for ensuring a strong, well-matched NIR. Samples 1-18 (Fig. 5) all fell within the targeted range. Sample 19 (Fig. 5d) fell slightly outside of the desired 20% by ±0.4%, as at very low diffraction efficiencies (<5%) it is increasingly difficult to successfully equalize the two holograms within this range. Furthermore, the acceptable range for equalization was very narrow at only ±~1%, therefore it was decided that sample 19 was included in the data.

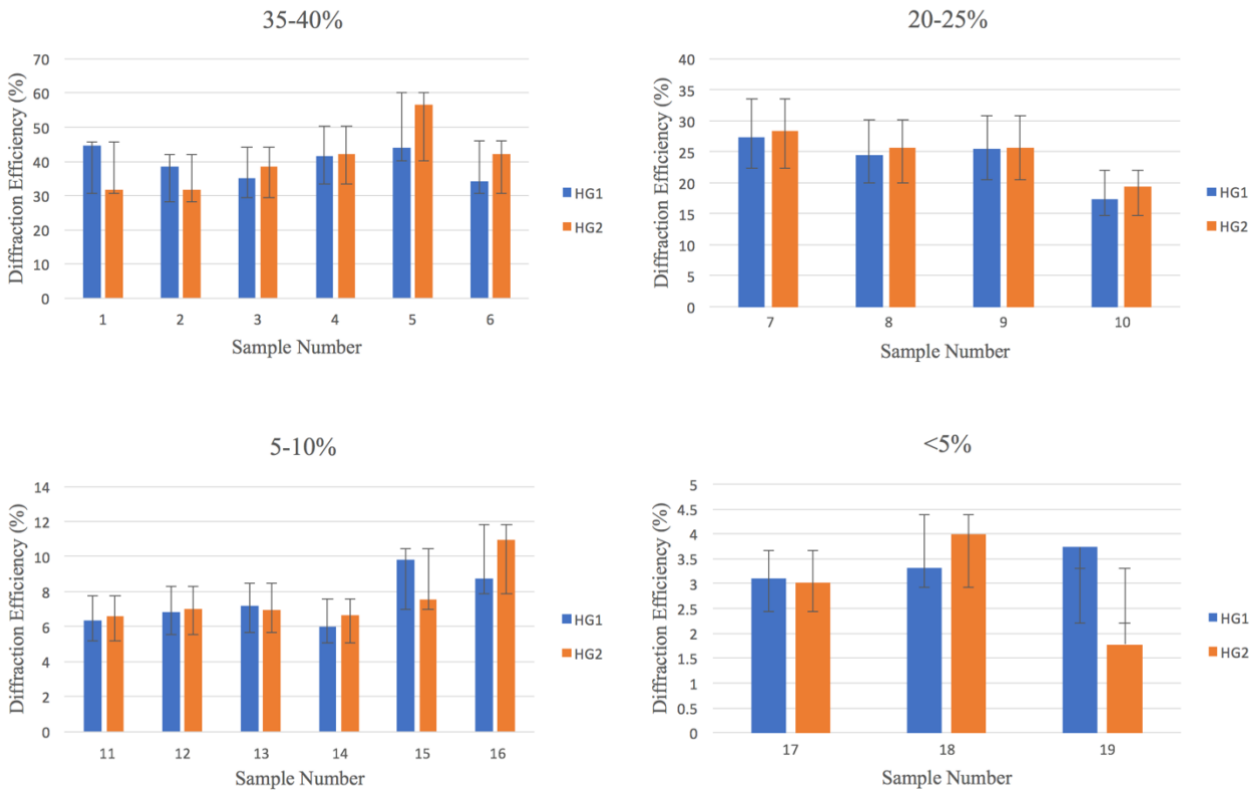

Figure 5(a-d). The diffraction efficiency of each HOE was measured in both output positions for HG1 and HG2 for samples with targeted efficiencies of (a) 35-40%; (b) 20-25%; (c) 5-10%; (d) <5%. The acceptable range for equalization of the diffraction efficiency of HG1 and HG2 is shown for each HOE.

A normalized intensity ratio was measured between the spots at HG1 and HG2 at both $L1_{min}$ and $L1_{max}$. In the $L1_{min}$ case, as expected, most of the probe beam was diffracted into the HG1 spot with some proportion of the light being transmitted and some being directed into the HG2 spot. Here we would expect an NIR value close to +1. In the $L1_{max}$ case, the opposite was expected and the probe beam was observed to be primarily diffracted into the HG2 spot, resulting in an NIR close to -1. The NIR of all samples is illustrated in Figure 6 and it can be seen that overall they were equal and opposite. The NIRs of samples 1 and 2 had the lowest values at ~0.5. This was probably a result of the relatively large mismatch in DE measured previously at HG1 and HG2, which was approximately 10%. An NIR of roughly 0.4 was also detected at the HG1 spot of samples 13 and 14, this may be due to low levels of light for these samples. However, in general a strong equal and opposite NIR was observed for samples with well-matched diffraction efficiencies. At HG1 an average NIR of 0.7, with a standard deviation of ± 0.15 was measured. An average NIR of -0.8 ± 0.12 was measured for HG2.

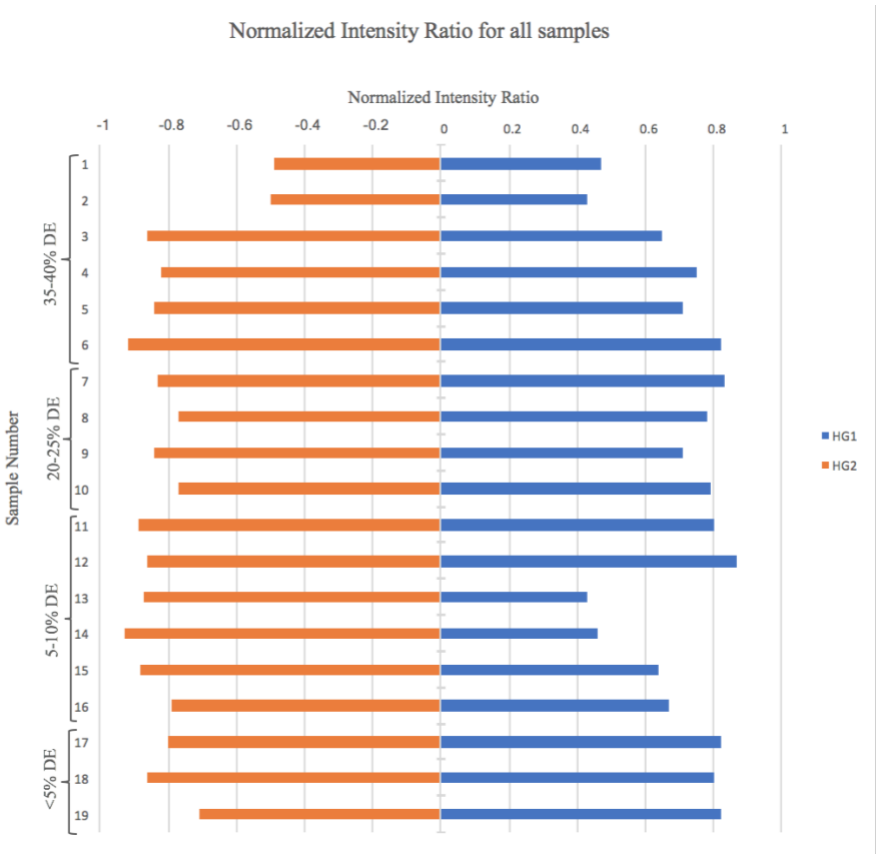

Figure 6. The normalized intensity ratio for all samples with targeted diffraction efficiencies of 35-40%, 20-25%, 5-10% and <5%.

3.2 Introduction of unknown defocus aberrations

A number of refractive lenses were chosen, with focal lengths 250mm (L2), 300mm (L3) and 400mm (L4), to introduce 'unknown' amounts of defocus onto the HOE. Each lens was positioned, along the rail in the reference arm, at a distance ("Lens to sample" - Table 1.) from the sample which ensured that the 4mm diameter of the HOE was perfectly matched. An aperture mounted in the reference arm allowed for the sample to be probed with a collimated beam also. A focus was formed behind the sample in the HG2 position before beginning to diverge. The distance from the sample to this focus was manually measured for each lens. The "Lens to sample" and "Sample to focus" distances were summed and the inverse of this sum was taken to express the total optical power in the system (HOE + lens contribution) in dioptres. Equation 6 was used to solve for the amount of defocus incident on the system, $1/f_1$, where f_2 is the focal length of the HOE itself (67mm) and d is the "Lens to sample" distance.

$$\text{Total optical power} = \frac{1}{f_1} + \frac{1}{f_2} - \frac{d}{f_1 f_2} \qquad \text{(Equation 6)}$$

Table 1. The lens to sample and sample to focus distances used to find the total optical power of the system. The amount of defocus incident on the sample was calculated for each 'unknown' aberration in dioptres.

Lens focal length (mm)	Lens to sample (d) (mm)	Sample to focus (mm)	Total optical power (dioptres)	Amount of defocus ($1/f_1$) (dioptres)
250	132 ± 0.5	30 ± 2	+6.2	+9.0 ± 0.1
300	159 ± 0.5	33 ± 2	+5.2	+7.1 ± 0.1
400	218 ± 0.5	40 ± 2	+3.9	+4.9 ± 0.1
Collimated beam	Inf	-	0	0

Four nominal amounts of the defocus aberration, +9.0D, +7.1D, +4.9D and 0D were classified, by all 19 HOEs with varying diffraction efficiency strengths (Fig. 7) by measuring the normalized intensity ratio produced when incident on the HOEs. As can be seen from Figure 7 , for HOEs with a targeted DE of 35-40% and 20-25%, all four aberrations were correctly measured to within an error of ~5% (Fig. 8), with most accurate results when identifying +4.9D, with an accompanying error of only 2.5%. Percentage error was calculated by taking an average of: (Amount of defocus - measured amount of defocus)/total detectable range (30D) x 100. Some positional inaccuracies of L2, L3 and L4 along the rail were to be expected, as placement of the lenses was carried out manually, which may have played a role in the higher percentage error that was consistently observed when measuring the +9.0D aberration. This issue could be avoided by generating the defocus aberration digitally with a spatial light modulator[16] or using electro-optomechanical positioning apparatus.

It was important to extend the study to include HOEs with low diffraction efficiencies as an indicator of the possible number of multiplexed aberration modes achievable. At a diffraction efficiency of 5%, it would be possible to multiplex a single HOE with up to 10 times a many 5% efficiency gratings as with a 50% grating, facilitating the simultaneous detection of many individual modes of aberration in one sensor. Encouraging success was seen for recordings in the 5-10% range, where an incident defocus aberration was consistently, correctly measured with a percentage error of approximately 5%. For HOEs with a DE <5%, 0D and +4.9D of defocus were correctly measured with a percentage error of <5%. Higher amounts of defocus, +7.1D and +9.0D, were measured to within an error of 5-10%. Given the large detectable range of 30.0D, the system was highly sensitive to very small changes in the intensity measured at HG1 and HG2. Lower measurable levels of light at low DE may account for some of the detection error introduced here. Decreasing the range of the system would increase the detection accuracy of the device while simultaneously reducing the sensitivity. For example, in applications in ophthalmology, it is expected that a range of ±6D would be sufficient for detecting the defocus aberration in most of the population. However, for other applications in adaptive optics the wider range of detection may be of benefit.

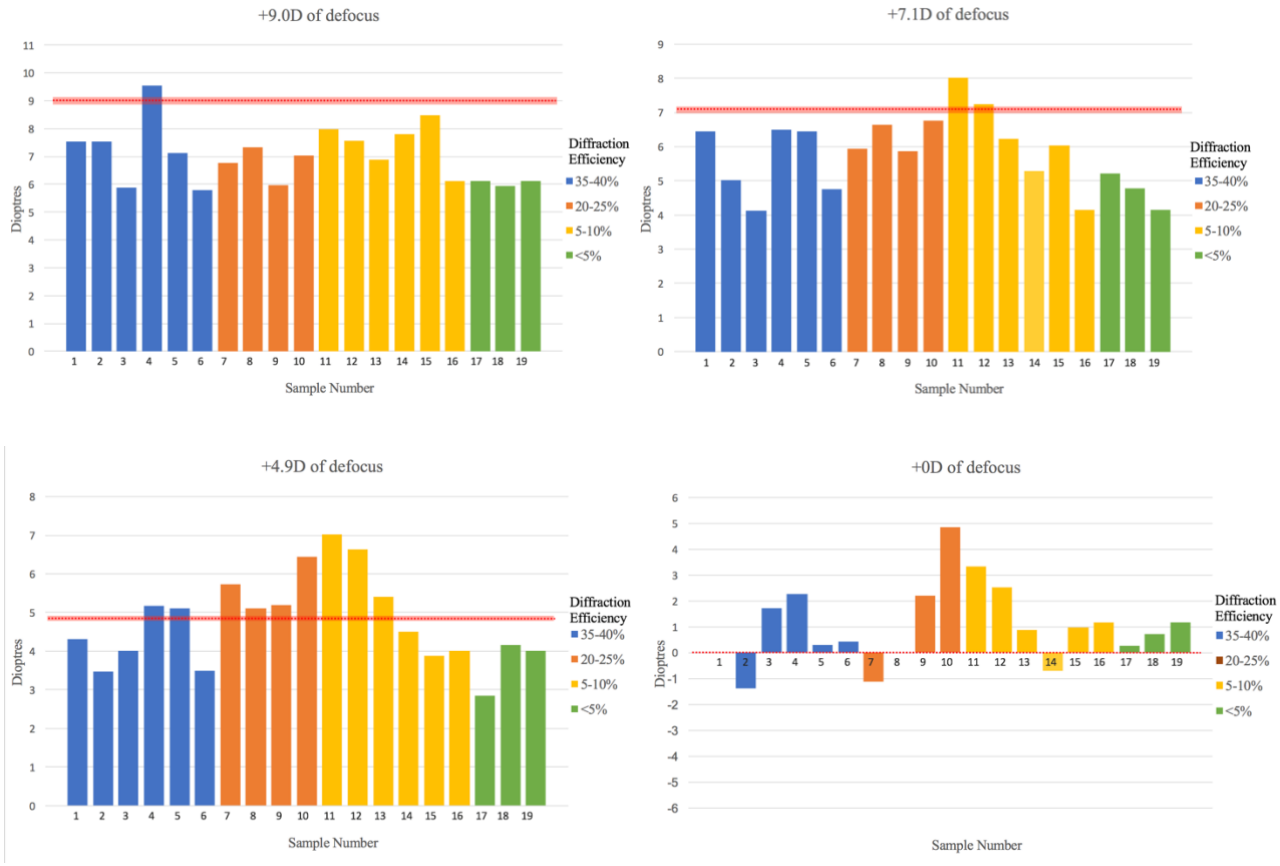

Figure 7(a-d). The amount of defocus calculated from NIRs detected by HOEs with varying diffraction efficiency strengths for (a) +9.0D; (b) +7.1D; (c) +4.9D; (d) 0D.

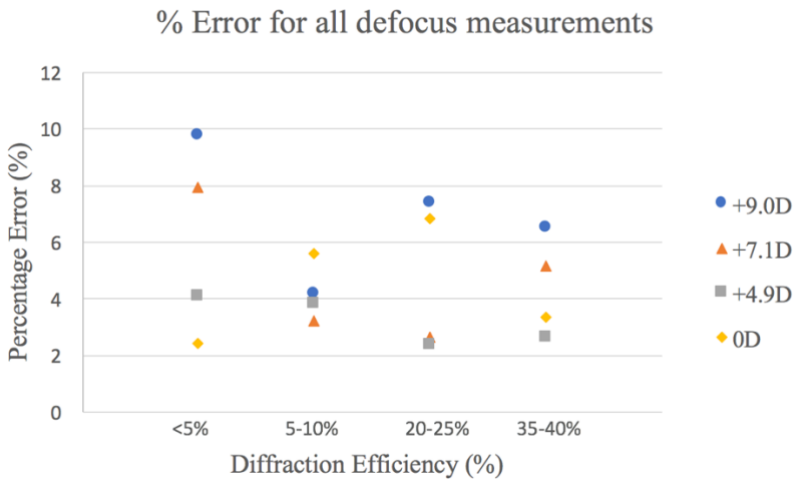

Figure 8. The percentage error associated with all defocus measurements carried out with HOEs with diffraction efficiencies of <5%; 5-10%; 20-25%; and 35-40%. Percentage error was calculated by taking an average of: (Amount of defocus - measured amount of defocus)/total detectable range (30D) x 100.

4. CONCLUSION

An analog holographic wavefront sensor was fabricated in an acrylamide-based photopolymer layer for the first time by using only conventional refractive elements in the recording process. This was achieved for a defocus aberration by multiplexing a maximum and minimum phase delay of a lens at two different carrier spatial frequencies (497 and 816 lines/mm). Good equalization of the diffraction efficiencies of HOEs was achieved to within 20% of the targeted DE for chosen ranges of 35-40%, 20-25%, 5-10 and <5%. Further work involving exposure scheduling of the recordings[17] will help to increase the accuracy of this equalization process. The results for targeted diffraction efficiencies of <5% are promising for extending the detection capabilities of the wavefront sensor to multiple aberration modes. It was seen that a strong equal and opposite normalized intensity ratio (0.7 to -0.8), between HG1 and HG2, could be achieved for HOEs with well-matched diffraction efficiencies. Varying amounts of defocus +9.0D, +7.1D, +4.9D and 0D were successfully identified to within ~5%, for HOEs with diffraction efficiencies as low as <5%.

Funding & Acknowledgements

This work was funded by Science Foundation Ireland (SFI) under grant award 18/SIRG/5666. The authors would also like to acknowledge the FOCAS Research Institute for equipment and technical support.

Author contributions

KM obtained the funding for the project and supervised project direction; KM, EB, SM & MS all contributed to the experimental plan; EB carried out all experimental work; EB, KM & SM contributed to the data analysis; EB produced all Figures; EB wrote the initial manuscript draft; KM, SM & MS edited the manuscript.

REFERENCES

[1] Geary, J. M., "Indirect Wavefront Measurement, Part II," [Introduction to Wavefront Sensors], 89–104 (1995).
[2] Platt, B. C. and Shack, R., "History and principles of Shack-Hartmann wavefront sensing," J Refract Surg **17**(5), S573-577 (2001).
[3] Liang, J., Williams, D. R. and Miller, D. T., "Supernormal vision and high-resolution retinal imaging through adaptive optics," J. Opt. Soc. Am. A **14**(11), 2884 (1997).
[4] Liang, J., Grimm, B., Goelz, S. and Bille, J. F., "Objective measurement of wave aberrations of the human eye with the use of a Hartmann–Shack wave-front sensor," JOSA A **11**(7), 1949–1957 (1994).
[5] Dai, G. (George)., "Ocular Wavefront Sensing and Reconstruction," [Wavefront Optics for Vision Correction], 97–129 (2008).
[6] Ting, C., Zhang, C. and Yang, Z., "Atmospheric free-space coherent optical communications with adaptive optics," Free-Space Laser Communication and Atmospheric Propagation XXIX **10096**, 1009606, International Society for Optics and Photonics (2017).
[7] Sun, H., Kasdin, N. J. and Vanderbei, R., "Efficient wavefront sensing for space-based adaptive optics," JATIS **6**(1), 019001 (2020).
[8] Kong, F. and Lambert, A., "Improvements to the modal holographic wavefront sensor," Applied Optics **55**, 3615 (2016).
[9] Andersen, G. P., Dussan, L. C., Ghebremichael, F. and Chen, K., "Holographic wavefront sensor," Optical Engineering **48**(8), 085801 (2009).
[10] Zepp, A., Gladysz, S. and Stein, K., "Holographic wavefront sensor for fast defocus measurement," Advanced Optical Technologies **2** (2013).
[11] Zepp, A., Gladysz, S., Stein, K. and Osten, W., "Optimization of the holographic wavefront sensor for open-loop adaptive optics under realistic turbulence Part I: simulations," Appl. Opt. **60**(22), F88 (2021).

[12] Neil, M. A. A., Booth, M. J. and Wilson, T., "New modal wave-front sensor: a theoretical analysis," J. Opt. Soc. Am. A **17**(6), 1098 (2000).
[13] Ghebremichael, F., Andersen, G. P. and Gurley, K. S., "Holography-based wavefront sensing," Applied Optics **47**(4), A62–A69 (2008).
[14] Vather, D., Naydenova, I., Cody, D., Zawadzka, M., Martin, S., Mihaylova, E., Curran, S., Duffy, P., Portillo, J., Connell, D., McDonnell, S. and Toal, V., "Serialized holography for brand protection and authentication," Applied Optics **57**(22), E131 (2018).
[15] Rogers, B., Martin, S. and Naydenova, I., "Study of the Effect of Methyldiethanolamine Initiator on the Recording Properties of Acrylamide Based Photopolymer," Polymers **12**(4), 734 (2020).
[16] Stein, K., Gladysz, S., Zepp, A., Anzuola, E. and Segel, M., "Novel wavefront strategies for strong atmospheric turbulence," January 2016.
[17] Naydenova, I., Akbari, H., Dalton, C., so Mohamed Ilyas, M. Y., Tee Wei, C. P., Toal, V. and Marti, S., "Photopolymer Holographic Optical Elements for Application in Solar Energy Concentrators," [Holography - Basic Principles and Contemporary Applications], E. Mihaylova, Ed., InTech (2013).